

Role of wave-particle resonance in turbulent transport in toroidal plasmas

G Dong^{1,*}  and Z Lin²

¹ Princeton Plasma Physics Laboratory, Princeton University, Princeton, NJ 08540, United States of America

² Department of Physics and Astronomy, University of California, Irvine, CA 92697, United States of America

E-mail: gdong@princeton.edu

Received 19 July 2021, revised 5 December 2021

Accepted for publication 13 December 2021

Published 21 January 2022



CrossMark

Abstract

A clear understanding of wave-particle interaction and associated transport mechanisms of different particle species in the drift wave instabilities is important for accurate modeling and predictions of plasma confinement properties in tokamaks. In particular, the roles of linear resonance and nonlinear scattering in turbulent transport need to be delineated when constructing reduced transport models. First-principle, global gyrokinetic simulations find that electron particle and heat transport decreases to a very low level, while ion heat transport level has no dramatic change when wave-particle resonance is suppressed in the collisionless trapped electron mode (CTEM) turbulence. On the other hand, ion heat transport in the self-consistent ion temperature gradient (ITG) turbulence simulation is qualitatively similar to that in the test-particle simulation using the static ITG turbulence fields. These simulation results show that electron transport is primarily driven by the wave-particle resonance in the CTEM turbulence, and the ion transport is mostly driven by the nonlinear wave-particle scattering in both the CTEM and ITG turbulence.

Keywords: turbulence, transport, tokamak, simulation

(Some figures may appear in colour only in the online journal)

1. Introduction

Turbulent transport in tokamak plasmas is often induced by microturbulence (Horton 1999) excited by unstable electrostatic drift waves such as ion temperature gradient (ITG) or collisionless trapped electron mode (CTEM) instabilities (Tang 1978). ITG instability can be driven by the ITG, which mainly cause ion heat loss. CTEM turbulence is linearly driven by the resonance between the drift-wave and the toroidal precession of the trapped electrons (Roach *et al* 1995), which causes electron heat and particle loss. While the nonlinear

saturation of the drift wave instability is typically a fluid process of wave-wave interactions such as self-regulation by zonal flows (Lin *et al* 1998, Dimits *et al* 2000) or nonlinear toroidal coupling (Chen *et al* 2005, Lin *et al* 2005), kinetic processes often dominate over fluid processes (e.g. eddy mixing) for the turbulent transport in the high-temperature fusion plasmas (Diamond *et al* 2010, Horton 2012, Weiland and Zagorodny 2019). In the nearly collisionless and wave-dominated electrostatic turbulence, transport carried by the random ExB drifts of charged particles can be regulated by the kinetic wave-particle decorrelation (Lin 2007a) or by the fluid eddy mixing (Xiao and Lin 2009, 2011) depending on the particle species and plasma regimes such as tokamak core (Rhodes *et al* 2002) or edge (Diallo and Laggner 2021). The

* Author to whom any correspondence should be addressed.

clear understanding of the wave-particle interaction and associated transport mechanisms of different particle species in the drift wave instabilities is important for accurate modeling and predictions of the plasma confinement properties in future tokamak devices such as ITER (ITER website, Hender *et al* 2007) and SPARC (SPARC website).

In the kinetic picture, the turbulent transport driven by the low-frequency microturbulence in the axisymmetric tokamak arises from breaking of one or both of the bounce (second, longitudinal) and the precession (third, toroidal canonical angular momentum) adiabatic invariants associated with guiding center quasi-periodic motions parallel and perpendicular, respectively, to the magnetic field lines (White 2001). In the collisionless plasmas, the breaking of the adiabatic invariants can be induced by either linear resonance of wave-particle interactions or nonlinear scattering of the guiding centers by the waves. The linear resonance occurs when wave frequency matches the guiding center bounce or precessional frequency, and the breaking of the adiabatic invariants is independent of the wave amplitude (Ishimaru 1978). The nonlinear scattering can induce nonlinear resonance, which can in turn regulate the nonlinear dynamics of the wave (Hahm and chen 1995). To achieve chaotic orbits through nonlinear scattering, the wave amplitude needs to be large enough for the breaking of adiabatic invariants, and the spatial scale of the turbulence eddy also affects the eddy rotation time and transport levels (Horton 1999, Lin *et al* 2002, Xiao and Lin 2009). The relative contributions of the linear resonance and nonlinear scattering could depend on both the specific resonance condition and turbulence intensity. The quasilinear transport models (Weiland and Zagorodny 2019) only take into account the linear resonance, but ignore the nonlinear scattering. Improved resonance broadened quasilinear models simplify the nonlinear effects in the wave-particle interaction processes as a broadening function for the resonance condition in the quasilinear operator (Berk *et al* 1995, Gorelenkov *et al* 2018). On the other hand, static turbulence fields are used to calculate test particle transport in some Monte-Carlo analyzes (Qin *et al* 2002, Kim *et al* 2017, Zhu *et al* 2018), which implicitly assume that nonlinear scattering dominates over linear resonance in driving the turbulent transport. These assumptions need to be verified in self-consistent simulations by treating both linear resonance and nonlinear scattering on an equal footing. For example, experimental profile predictions using quasi-linear transport model is found inadequate for quantitative comparison with ITER-relevant JET experimental results (Garcia *et al* 2019).

Here we study the relative importance of the two mechanisms for ions and electrons by comparing transport levels driven by self-consistent microturbulence and by static turbulence fields recorded from self-consistent gyrokinetic simulations (Lee 1983, Brizard and Hahm 2007). In this work, we study the linear and nonlinear wave-particle interactions in the ITG and CTEM turbulences in the tokamak. First-principles global gyrokinetic simulations of electrostatic ITG and CTEM turbulence are carried out using gyrokinetic toroidal code (GTC), which has extensively been applied to study the microturbulences (Lin *et al* 1998, Lin *et al* 2007a, Xiao and Lin 2009), energetic particle turbulent transport (Zhang *et al* 2008,

2012), and kinetic MHD turbulences (Dong *et al* 2019) in core and edge plasmas (Xie *et al* 2017). Linear resonance is driven by frequency matching between the wave and particle orbital motion, and can be suppressed when the turbulence fields are set static with zero frequency. Particle scattering effects are still present in static fields as long as the spatial variation of the fields are unchanged. To study the relative contributions of the linear resonance and nonlinear scattering, we compare the turbulent transport in the fully self-consistent ITG and CTEM turbulence simulations incorporating both transport mechanisms and in test-particle simulations that suppress the wave-particle resonance by using static turbulence fields. Simulation results show that in the CTEM turbulence, when wave-particle resonance is suppressed, electron heat and particle transport decreases to a very low level, while ion heat transport level has no dramatic change. Similarly, ion heat transport in the test-particle simulation using the static ITG turbulence fields also exhibits only quantitative difference from that in the self-consistent ITG turbulence simulation. These simulation results show that electron transport is primarily driven by the wave-particle precessional resonance in the CTEM turbulence, but the ion transport is mostly regulated by the nonlinear wave-particle scattering in both the CTEM and ITG turbulence.

These findings can be useful in transport analysis and predictions in the plasma core and edge. More importantly, the physics picture of electron and ion transport mechanisms in the ITG and CTEM turbulence can help in designing and validating the models for turbulent transport in tokamak plasmas. For example because electrons can stay persistently in the precessional resonance due to the weak radial dependence of the precessional frequency, electron transport in the CTEM turbulence is fluid-like, which cannot be modeled accurately by the quasilinear theory (Xiao and Lin 2009). Transport mechanisms in the ITG and CTEM turbulence are studied in sections 2 and 3, respectively. Section 4 is the summary.

2. ITG turbulence

Gyrokinetic simulations using GTC utilize particle-in-cell methods to calculate the wave particle interactions with full non-local and kinetic effects. At each time step in the simulations, the particle equations of motion are solved along with the perturbed gyrokinetic equation and Poisson's equation for the perturbed electrostatic field. To study the ITG turbulence, the global GTC simulations use representative tokamak plasmas with concentric flux-surfaces and the following local parameters at a radial position $r = 0.5a$, $R/L_{Ti} = 6.9$, $R/L_n = 2.2$, $q = 1.4$, $s = 0.78$, $T_e/T_i = 1$ and $a/R = 0.36$. Here, R and a are the major and minor radii, L_{Ti} and L_n are the ion temperature and density gradient scale lengths, T_i and T_e are the ion and electron temperatures, respectively, q is the safety factor and s is the magnetic shear. The profile for the safety factor is $q = 0.581 + 1.092(r/a) + 1.092(r/a)^2$ and for the temperature and density gradients is $\exp\{-[(r - 0.5a)/0.32a]^6\}$. The boundary condition of the perturbed electrostatic potential $\delta\phi$ is enforced at $r < 0.1a$ and $r > 0.9a$. The size of the tokamak

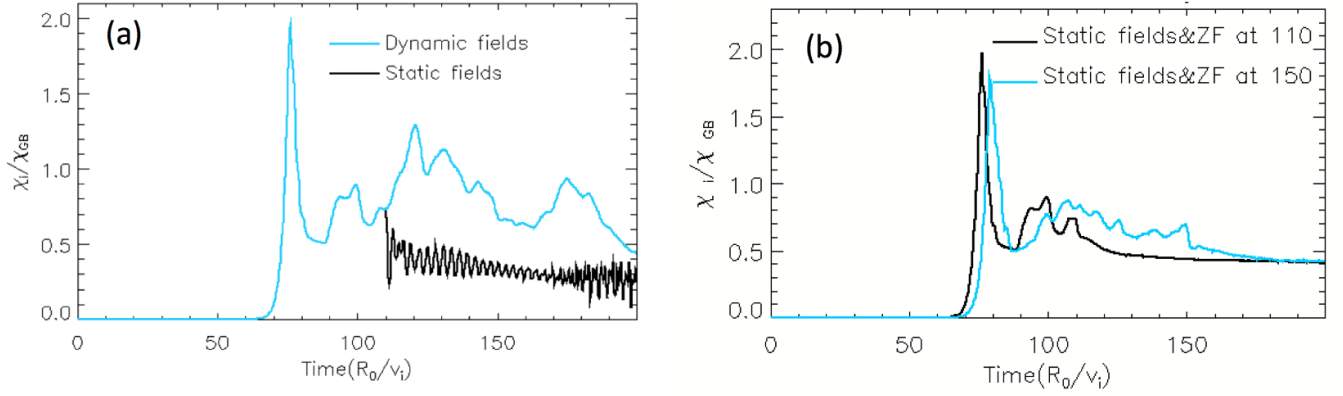


Figure 1. Time history of ion heat conductivity χ_i with self-consistent dynamic fields (blue) and static non-zonal fields (black) in the nonlinear regime are shown in (a). The ion heat conductivity from the static fields is reduced by around a factor of two compared with that from the self-consistent fields. Panel (b) shows χ_i in two simulations with static non-zonal fields and zonal flow since earlier (black) and later (blue) time in the nonlinear regime.

used in the simulation is $a = 250\rho_i$, where $\rho_i = v_i/\Omega_i$ is the ion gyroradius, $v_i = (T_i/m_i)^{1/2}$ is the ion thermal speed, Ω_i is the ion gyrofrequency, and m_i is the ion mass. The GTC global field-aligned mesh consists of 64 parallel grids and a set of unstructured radial and poloidal grids with a perpendicular grid size of ρ_i . The time step is $0.2L_{Ti}/v_i$. In the ITG simulations, ions are governed by the gyrokinetic equation (Brizard and Hahm 2007) and electrons are assumed to be adiabatic.

In the self-consistent nonlinear electrostatic simulations using the plasma parameters described above, the ITG is the dominant instability. The time evolution of the ITG-induced transport is shown in figure 1 in the solid blue line. The self-consistent heat flux $q = \int d^3v (\frac{1}{2}mv^2 - \frac{3}{2}T) \delta v_{E \times B} \delta f$ is used to define the effective ion heat conductivity χ_i by using the relation $q = -n_0 \chi \nabla T$, where v is the particle velocity, $\delta v_{E \times B}$ is the radial component of the gyroaveraged ExB drift, and δf is the perturbed particle distribution function. The ITG instability first grows exponentially in the linear regime until around $t = 70 R_0/v_i$, and then saturates due to the self-regulation by zonal flows. Finally, the turbulence is fully developed and the ion heat conductivity reaches an amplitude on the order of the gyro-Bohm level ($\chi_{GB} = \rho_i^2 v_i/a$). The particle flux is zero since electron response is adiabatic.

To delineate the relative contributions of the linear and nonlinear effects on transport, we compare the transport between fully self-consistent simulation and test-particle simulation with fixed turbulence fields. In the test-particle simulation, we record the turbulence fields and all particle information at $t = 110 R_0/v_i$ from the fully self-consistent simulation and restart the simulation with the fixed turbulence fields. The particles are reloaded according to their weight (perturbed distribution function), coordinates and velocity when the fields are fixed. The resulting ion heat conductivity is shown in black solid line in figure 1(a). We find that the ion heat conductivity from the fixed fields changes quantitatively, around a factor of 2, compared with that from the self-consistent dynamic fields, as shown in figure 1(a). To prevent large unphysical ion particle flux (charge separation), zonal flows are kept self-consistently, which induce the geodesic acoustic mode (GAM)

oscillation with a frequency of $\omega \sim 2.3v_i/R_0$. The observed GAM frequency is in agreement with the earlier theory (Zonca and Chen 2008) and simulation (Hallatschek and Biskamp 2001). To test the role of the self-consistent zonal flows, we perform the same simulations of the ITG turbulence by fixing both the zonal flow and the non-zonal components of the turbulence fields. The change in ion heat flux is qualitatively the same, as shown in figure 1(b). In the following context, ‘fixed fields’ and ‘static fields’ refer to the static non-zonal component of the turbulence fields. Note that we chose a restart time to fix the fields after the turbulent transport level saturates. When we pick a different restart time to freeze the turbulence fields, the simulation results are qualitatively the same for ITG. Figure 1(b) also shows an ITG simulation with slightly different initial conditions and different restart time at around $t = 150 R_0/v_i$, where both zonal and non-zonal components become static.

To verify that the test particle transport is induced by the ExB scatterings, we examine the phase space structure of χ_i , for the self-consistent and test-particle simulations in figure 1(a). Since ion transport is diffusive in the ITG turbulence, the phase space structure of the ion heat conductivity can be calculated accurately through the ion mobility D_{eff} , defined as:

$$D_{eff} = \frac{1}{2N\Delta t} \sum_{i=1}^N \Delta r_i^2, \quad (1)$$

where $\Delta r_i = r_i(t + \Delta t) - r_i(t)$ is the radial displacement of the guiding centers, and $i = [1, N]$ denotes the particle label. Equation (1) is valid for any time separation Δt that is longer than the effective wave-particle decorrelation time. Time history of D_{eff} is indeed proportional to the ion heat conductivity χ_i , which further verifies the diffusive nature of the ion transport.

Figure 2 shows the phase space (E, λ) structure of the ion mobility averaged over $\Delta t = 25 R_0/v_i$ in the nonlinear regime of the ITG turbulence with self-consistent fields (panel a) and with fixed fields (panel b), color scale represents D_{eff} .

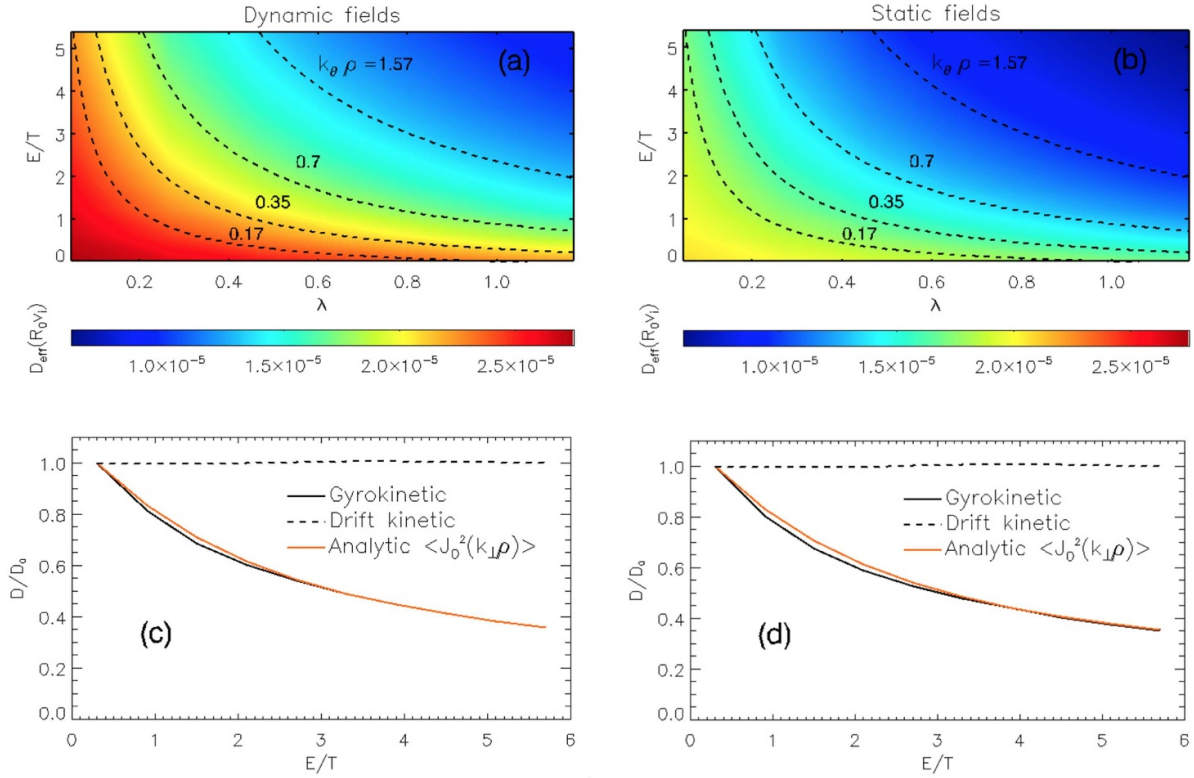


Figure 2. Phase space (E, λ) structure of ion mobility D_{eff} in the ITG nonlinear regime with self-consistent fields (a) and with fixed fields (b). The dashed black lines represent constant $k_\theta \rho$ values. The phase space cut for the deeply trapped particles is shown solid black line in panels (c) and (d) in the self-consistent field and fixed field respectively, demonstrating good agreement with analytic results of the gyro-averaging (red line). Drift kinetic test particle mobility is also shown in dashed line in panels (c) and (d).

Here, $\lambda = \mu B_0/E$ is a pitch-angle ξ related variable, where B_0 is the equilibrium on axis magnetic field, and $\xi = v_{\parallel}/v$. We find that the constant D_{eff} curves in the (E, λ) phase space fit very well to the constant- $k_\theta \rho$ curves for both the self-consistent fields and the fixed fields. This indicates that the breaking of the constants of motion in both cases is due to the ExB drifts, which exhibits the phase space structure only in the form of $k_\theta \rho$ through the gyro-averaging of the turbulence fields. To further verify that the structure of panels (a) and (b) comes from the gyro-averaging for the gyrocenters, we take a cut of the (E, λ) phase space for the deeply trapped particles with $-0.1 < \xi < 0.1$. Panels (c) and (d) show that the ion mobility (black curves) fits almost perfectly with the analytic results of the gyro-averaging (red curves), i.e., the square of the Bessel function $\langle J_0^2(k_\perp \rho) \rangle / \langle J_0^2(k_\perp \rho_0) \rangle$ for both the self-consistent fields and the fixed fields. Here $k_\perp = \sqrt{k_\theta^2 + k_r^2}$ is the perpendicular wave number and $\langle \dots \rangle$ is average over the poloidal field spectrum. k_θ and k_r are chosen with fixed weight in this calculation according to the 1D poloidal and toroidal spectrum. Figure 3 shows the 1D poloidal and radial spectrums for ITG in panel (a) and CTEM in panel (b). Since in ITG turbulence the average k_r is much smaller than k_θ , rendering the correction from k_r to k_\perp very small. In the CTEM turbulence discussed in the next section, $k_r/k_\theta \sim 0.6$, as shown in panel (b) of figure 3, bringing a 20% correction to k_\perp . Furthermore, we measured the

ion mobility by using test guiding centers without the gyro-averaging processes. These test guiding centers do not feed back to the turbulence fields, and therefore do not affect the turbulence dynamics. The ion mobility measured from the test guiding centers shown in dashed curves in panels (c) and (d) of figure 2 is indeed almost uniform in both self-consistent fields and in fixed fields. The phase space structure of the gyrocenter mobility only come from the gyro-averaging, and the guiding center mobility is independent of the kinetic energy. The excellent fitting by the $J_0^2(k_\theta \rho)$ function indicates that the second (bounce) invariant of the ion is broken by the nonlinear ExB drifts, which still allows gyro-averaging effects. The drift-bounce resonance (Chen 1999) is not important for the ions with thermal energy, so that there is no guiding center orbit averaging effects (Zhang and Lin 2013). This is consistent with the fact that the ITG linear growth rate is larger than the ion bounce frequency.

These results show that the ion transport in the ITG turbulence is dominated by the nonlinear ExB scattering, due to the breaking of the longitudinal invariant. The linear and nonlinear resonances due to the time variations of the turbulence fields is subdominant. We conjecture that the nonlinear resonance is weaker than the linear resonance or nonlinear scattering since the ITG instability saturation is primarily due to zonal flow regulation, which significantly reduces the ITG turbulence intensity (Lin *et al* 1998).

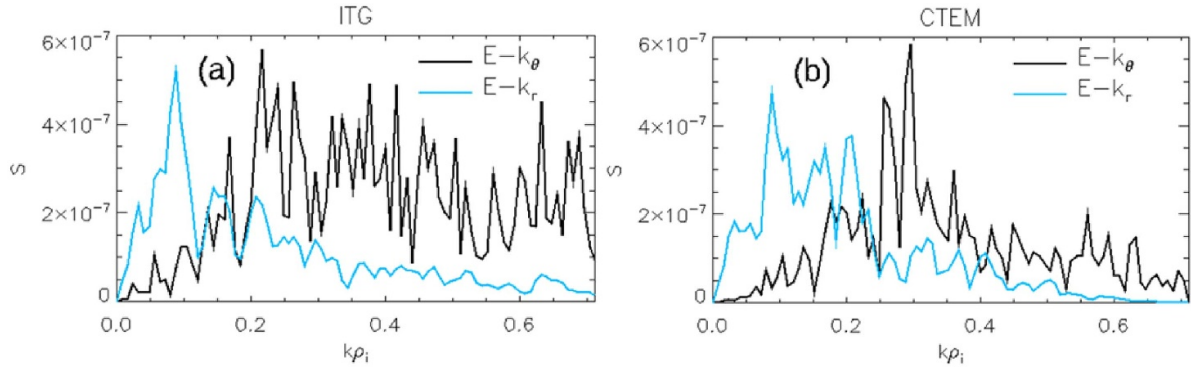


Figure 3. ITG (a) and CTEM (b) turbulence poloidal (black) and radial (blue) spectrum S .

3. CTEM turbulence

To study the CTEM turbulence, we use the plasma parameters described above but with the ITG of $R_0/L_{Ti} = 2.2$ and electron temperature gradient of $R/L_{Te} = 6.9$. For these parameters, the wave propagation is in the electron direction, and the linear mode structure is consistent with CTEM features, showing that the CTEM is the dominant instability (Xiao and Lin 2009). The trapped electrons dynamics are simulated by the drift kinetic equation using the fluid-kinetic hybrid electron model (Lin *et al* 2007b) and the passing electrons are assumed to be adiabatic. The time evolution of the CTEM-induced electron heat transport, ion heat transport and particle transport from the simulation is shown in figure 4. The self-consistent particle flux $\Gamma = \int dv^3 \delta v_{E \times B} \delta f$ is used to define the particle diffusivity D by using the relation $\Gamma = -D \nabla n$. The CTEM instability initially grows exponentially in the linear regime, with linear growth rate $\gamma^{lin} = 0.55 v_i/R_0$. At $t = 50 R_0/v_i$, the mode reaches a nonlinear regime when the radial averaged electrostatic potential $\frac{e \delta \phi_{rms}}{T_e} \sim 0.01$. In the nonlinear regime, electron heat flux, ion heat flux, and particle flux saturate around $t = 60-80 R_0/v_i$ to reach a fully developed turbulence.

In the wave-dominated turbulence, electron transport is induced by the breaking of the precession adiabatic invariants mostly by linear resonance due to the time variations of the fluctuating fields. The nonlinear scattering of electron banana orbits cannot break the longitudinal invariant, but lead to a much weaker radial de-tuning, where trapped electron precessional frequency changes slowly when the banana orbit moves across the flux-surface (Xiao and Lin 2011). To verify the dominance of the linear resonance, we compare the transport between fully self-consistent simulation with dynamic fields and test-particle simulation with fixed turbulence fields at $t = 80 R_0/v_i$. We find that the electron transport levels rapidly decrease with GAM oscillations after the fields are fixed. The electron heat conductivity in figure 4(a) and particle diffusivity in figure 4(c) eventually drop to a very low level with fixed turbulence fields, indicating the dominance of the linear resonance in driving the electron transport. The relaxation

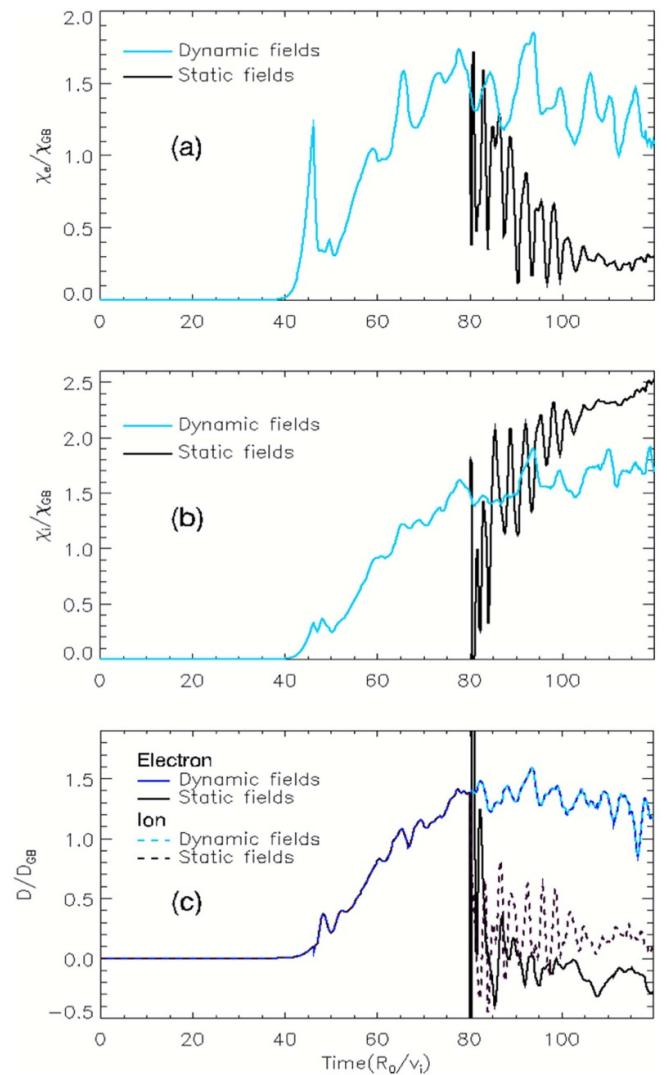


Figure 4. Time history of (a) electron heat conductivity χ_e , (b) ion heat conductivity χ_i , and (c) particle diffusivity D with self-consistent dynamic fields (blue lines) and with fixed fields in the nonlinear regime (black lines). Electron heat and particle transport drops to a very low level when fields are fixed, while ion heat transport level changes only slightly.

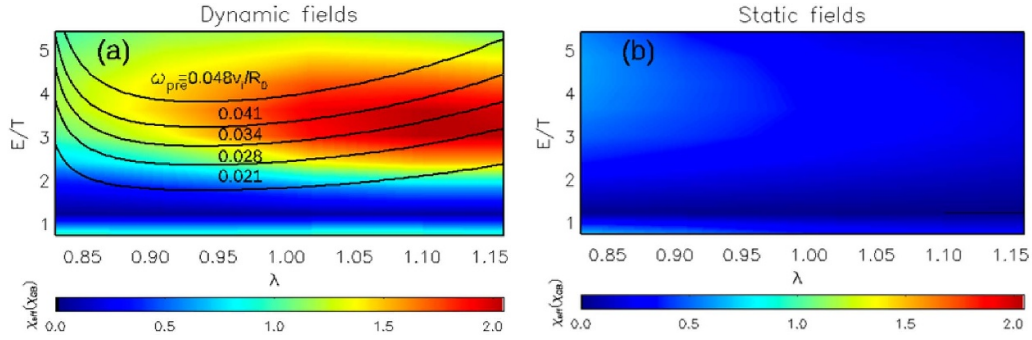


Figure 5. Electron mobility χ_{eff} in 2D phase space (E, λ) (a) in the nonlinear stage with self-consistent fields and (b) with fixed fields. The black lines in (a) represent the electron precessional frequency.

time of the transport levels is around $15 R_0/v_i$, which is determined by the orbital phase mixing time, approximately equal to the CTEM wave period. With the static electric fields, most of the electron orbits are confined due to the conservation of energy, magnetic moment, and longitudinal invariant. On the other hand, the ion heat conductivity from the fixed turbulence fields changes only quantitatively, within a factor of 2 compared with that from the self-consistent fields, suggesting that the ExB scattering dominates the ion nonlinear dynamics in CTEM turbulence, where the ion longitudinal invariant is broken by the nonlinear ExB drift. When we pick a different restart time to freeze the CTEM turbulence fields, the heat and particle transport changes are qualitatively the same.

In the test-particle simulations, the turbulence autocorrelation time is infinity. The autocorrelation time is longer than the dominant timescale of the decorrelation process underlying transport, for example the eddy rotation time in the CTEM and the wave-particle decorrelation time in the ITG turbulence (Xiao and Lin 2009). Therefore, eliminating the turbulence auto-decorrelation should not affect the electron and ion transport qualitatively. The lack of temporal decorrelation may explain quantitative differences of the ion transport between self-consistent simulations and test-particle simulations of the ITG and CTEM turbulence. Furthermore, in the ITG simulations, electrons are adiabatic, so there is no particle transport. On the other hand, in CTEM simulations, ion particle transport level is the same as the electron particle transport level due to the quasi-neutrality condition. This difference in the ion particle transport may also cause quantitative differences in the ion transport in the CTEM and ITG turbulence.

In figure 4, the ion and electron particle diffusivity are identical to the self-consistent turbulence fields as expected from the quasi-neutrality condition, but has a small difference in the residues with fixed turbulence fields, which can be caused by the breaking of quasi-neutrality condition when the gyrokinetic Poisson's equation (i.e. quasi-neutrality condition) is no longer solved when the non-zonal component of the electrostatic potential is fixed. To test the role of the self-consistent zonal flows, we perform the same simulations of the ITG and CTEM turbulence by fixing both the zonal flow and the non-zonal components of the turbulence fields. The electron and ion heat transport evolves in a similar trend without the GAM oscillation. In the CTEM turbulence, ion particle flux remains

a finite value, and deviates dramatically from electron particle flux.

To further verify the importance of the linear resonance and nonlinear scattering in driving electron and ion transport, respectively, we study the phase space structures of ion and electron mobility. We continue to use (E, λ) as the phase space coordinate for ions and electrons. For trapped electrons, $1 - \varepsilon < \lambda < 1 + \varepsilon$. In this diagnosis, ions and electrons are selected from around the $r = 0.5a$, therefore $\varepsilon = r/R_0 \approx 0.18$, and $0.82 < \lambda < 1.18$. For both species there are 10 bins in each dimension, and more than 5000 particles in each bin. For enhanced statistics all the values are averaged over a time period of $25R_0/V_i$.

In the CTEM turbulence, trapped electron motion is not purely diffusive (Xiao and Lin 2011), and the mobility calculated in equation (1) is no longer a good representation for the heat conductivity and particle diffusivity. Therefore, we use the effective heat conductivity defined as $\chi_{eff} = q(E, \lambda)T/(n_0 \nabla T E)$ to represent the phase space distribution of the heat conductivity by using the heat flux at a local phase space position. The distribution of the electron effective heat conductivity in the nonlinear stage in figure 5(a) is consistent with previous CTEM simulation results using Lagrangian analysis (Xiao and Lin 2011), which verifies that χ_{eff} is a proper substitute for trapped electron transport.

Figure 5(a) indicates that before freezing the fluctuating fields, electron heat transport mainly comes from the contribution of deeply trapped particles around the energy $\sim 4T_e$. The resonance condition for a trapped particle is $\omega = n\omega_{pre} + p\omega_b$, in which ω is the real frequency of the field, ω_{pre} and ω_b are the precessional and bounce frequency, and n is the toroidal mode number. Take $p = 0$ since electron bounce motion is much faster than the CTEM frequency, we can get the precessional resonance condition $\omega = n\omega_{pre}$. The linear CTEM frequency is nearly dispersiveless, with $\omega^{lin} = 1.52 k_\theta \rho_i v_i / R_0 = 0.017 n v_i / R_0$ for the range of $0 < k_\theta \rho_i < 1$. The nonlinearly dominant mode is $k_\theta \rho_i = 0.3$ with $n = 27$ in the nonlinear regime. This gives $\omega/n = 0.034 v_i / R_0$, which is consistent with the mobility distribution in figure 5(a). We note that the nonlinear CTEM frequency is about twice the linear CTEM frequency. The physics of this nonlinear CTEM frequency shift will be investigated in future study. After the fields are fixed, the distribution became almost uniform with small values, as

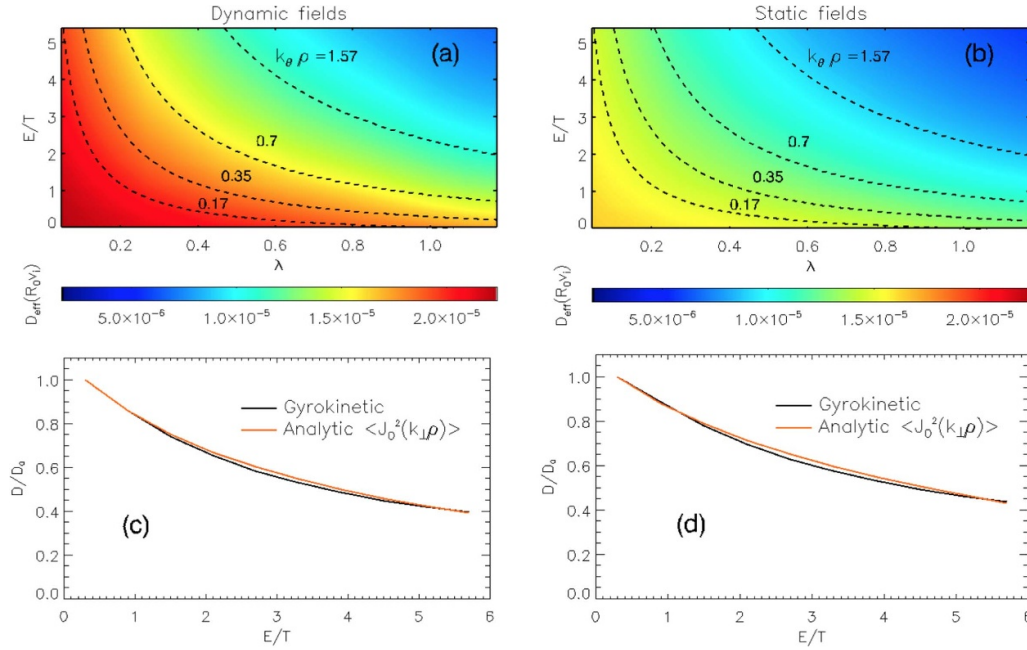


Figure 6. Ion mobility D_{eff} in the CTEM turbulence with self-consistent field (a) in 2D phase space and (c) for the deeply trapped particles and with fixed field (b) in 2D phase space and (d) for the deeply trapped particles. The black lines in both (a) and (b) represent fixed $k_{\theta}\rho$ values.

shown in figure 5(b). This is also consistent with our observation in figure 4, which indicates that the electron transport due to the nonlinear ExB drifts is very small because of the conservation of the longitudinal invariants. The structure of the ion mobility is shown in figure 6, which exhibits similar features as observed in the ITG turbulence, and indicates that the ion bounce invariant is also broken by the nonlinear ExB drifts in the CTEM turbulence. However, we note that in the CTEM simulations the phase space integrated ion mobility does not exactly match the measured heat conductivity, indicating that the ion species are not purely diffusive in the CTEM turbulence.

4. Conclusions

In this work, the effect of wave-particle resonance on turbulent transport in fusion plasmas is studied using global gyrokinetic particle simulations of the ITG and CTEM turbulence. To summarize the results from CTEM and ITG simulations, electron transport is primarily driven by wave-particle resonance, and the ion transport is driven by nonlinear wave-particle scattering. For trapped electrons, since the nonlinear decorrelation is weak (Xiao and Lin 2009), the first and second adiabatic invariants (μ , J_{\parallel}) are conserved, and the linear precessional resonance (with the resonance condition $\omega = n\omega_{pre}$) breaks the precession adiabatic invariant (toroidal canonical angular momentum), which induces the radial transport. After the field is fixed in the simulation, $\omega = 0$, the electron transport reduces greatly due to the removal of the linear and nonlinear resonance. The nonlinear frequency associated with ExB drift might induce small transport by breaking the precession invariant. When the turbulence fields are fixed, the ion transport levels do

not encounter qualitative change. These results might be able to explain the strong linear resonance observed in the transport of trapped electrons, and weak linear resonance observed in the transport of ions. Although in the simulations presented here, the measured transports are from the thermal species in the ITG and CTEM turbulence, the transport mechanisms apply to any species including the energetic particles, in terms of breaking of the constants of motion. Therefore, the physics discussed here is applicable to any species, but depending on wave-particle resonance channel. The modeling of turbulent transport in new experimental scenarios and future tokamaks is a complicated integrated task that depends strongly on the specific geometry and plasma parameters. Reduced models (e.g. Monte Carlo codes using fixed turbulence fields) need to be verified by first-principle codes for the prediction of transport levels. The findings reported in this paper confirm the different transport mechanisms for different species in the ITG and CTEM turbulence, and can help verify the validity and applicability of analytical and computational tools for modeling the particle and heat transport in present and future toroidal plasma devices.

Data availability statement

All data that support the findings of this study are included within the article (and any supplementary files).

Acknowledgments

This work was supported by US Department of Energy (DOE) SciDAC ISEP Center. Research at the Princeton

Plasma Physics Laboratory is supported by the US DOE Contract DE-AC02-09CH11466. This work used resources of the Oak Ridge Leadership Computing Facility at Oak Ridge National Laboratory (DOE Contract No. DE-AC05-00OR22725) and the National Energy Research Scientific Computing Center (DOE Contract No. DE-AC02-05CH11231).

ORCID iD

G Dong  <https://orcid.org/0000-0002-7734-3736>

References

- Berk H L, Breizman B N, Fitzpatrick J and Wong H V 1995 Line broadened quasi-linear burst model *Nucl. Fusion* **35** 1661
- Brizard A and Hahm T S 2007 Foundations of nonlinear gyrokinetic theory *Rev. Mod. Phys.* **79** 421
- Chen L 1999 Theory of plasma transport induced by low-frequency hydromagnetic waves *J. Geophys. Res.* **104** 2421
- Chen L, Zonca F and Lin Z 2005 Nonlinear toroidal mode coupling: a new paradigm for drift wave turbulence in toroidal plasmas *Plasma Phys. Control. Fusion* **47** B71
- Diallo A and Lagner F M 2021 Review: turbulence dynamics during the pedestal evolution between edge localized modes in magnetic fusion devices *Plasma Phys. Control. Fusion* **63** 013001
- Diamond P H, Itoh S-I and Itoh K 2010 *Modern Plasma Physics: Volume 1, Physical Kinetics of Turbulent Plasmas* 1st edn (Cambridge: Cambridge University Press)
- Dimits A M *et al* 2000 Comparisons and physics basis of tokamak transport models and turbulence simulations *Phys. Plasmas* **7** 969–83
- Dong G, Bao J, Bhattacharjee A and Lin Z 2019 Nonlinear saturation of kinetic ballooning modes by zonal fields in toroidal plasmas *Phys. Plasmas* **26** 010701
- Garcia J *et al* 2019 First principles and integrated modelling achievements towards trustful fusion power predictions for JET and ITER *Nucl. Fusion* **59** 086047
- Gorelenkov N N, Duarte V N, Podesta M and Berk H L 2018 Resonance broadened quasi-linear (RBQ) model for fast ion distribution relaxation due to Alfvénic eigenmodes *Nucl. Fusion* **58** 082016
- Hahm T S and Chen L 1995 Nonlinear saturation of toroidal Alfvén eigenmodes via ion Compton scattering *Phys. Rev. Lett.* **74** 266
- Hallatschek K and Biskamp D 2001 Transport control by coherent zonal flows in the core/edge transitional regime *Phys. Rev. Lett.* **86** 1223
- Hender T C *et al* 2007 Chapter 3: MHD stability, operational limits and disruptions *Nucl. Fusion* **47** S128
- Horton W 1999 Drift waves and transport *Rev. Mod. Phys.* **71** 735
- Horton W 2012 *Turbulence Transport in Magnetized Plasmas* (Singapore: World Scientific)
- Ishimaru A 1978 *Wave Propagation and Scattering in Random Media* vol 2 (New York: Academic Press)
- ITER organization 2021 *ITER—Unlimited Energy* (available at: www.iter.org/) (Accessed 17 July 2021)
- Kim H-T, Romanelli M, Yuan X, Kaye S, Sips A C C, Frassinetti L and Buchanan J 2017 Statistical validation of predictive TRANSP simulations of baseline discharges in preparation for extrapolation to JET D–T *Nucl. Fusion* **57** 066032
- Lee W W 1983 Gyrokinetic approach in particle simulation *Phys. Fluids* **26** 556
- Lin Z, Chen L and Zonca F 2005 Role of nonlinear toroidal coupling in electron temperature gradient turbulence *Phys. Plasmas* **12** 056125
- Lin Z, Ethier S, Hahm T S and Tang W M 2002 Size scaling of turbulent transport in magnetically confined plasmas *Phys. Rev. Lett.* **88** 195004
- Lin Z, Hahm T S, Lee W W, Tang W M and White R B 1998 Turbulent transport reduction by zonal flows: massively parallel simulations *Science* **281** 1835
- Lin Z, Holod I, Chen L, Diamond P H, Hahm T S and Ethier S 2007a Wave-particle decorrelation and transport of anisotropic turbulence in collisionless plasmas *Phys. Rev. Lett.* **99** 265003
- Lin Z, Nishimura Y, Xiao Y, Holod I, Zhang W L and Chen L 2007b Global gyrokinetic particle simulations with kinetic electrons *Plasma Phys. Control. Fusion* **49** B163
- PSFC MIT Plasma Science and Fusion Center *SPARC* (available at: www.psfc.mit.edu/sparc) (Accessed 17 July 2021)
- Qin G, Matthaeus W H and Bieber J W 2002 Perpendicular transport of charged particles in composite model turbulence: recovery of diffusion *Astrophys. J.* **578** L117–20
- Rhodes T L *et al* 2002 Comparison of turbulence measurements from DIII-D low-mode and high-performance plasmas to turbulence simulations and models *Phys. Plasmas* **9** 2141
- Roach C M, Connor J W and Janjua S 1995 Trapped particle precession in advanced tokamaks *Plasma Phys. Control. Fusion* **37** 679
- Tang W M 1978 Microinstability theory in tokamaks *Nucl. Fusion* **18** 1089
- Weiland J and Zagorodny A 2019 Drift wave theory for transport in tokamaks *Rev. Mod. Plasma Phys.* **3** 8
- White R B 2001 *The Theory of Toroidally Confined Plasmas* 2nd edn (London: Imperial College Press)
- Xiao Y and Lin Z 2009 Turbulent transport of trapped-electron modes in collisionless plasmas *Phys. Rev. Lett.* **103** 085004
- Xiao Y and Lin Z 2011 Convective motion in collisionless trapped electron mode turbulence *Phys. Plasmas* **18** 110703
- Xie H S, Xiao Y and Lin Z 2017 New paradigm for turbulent transport across a steep gradient in toroidal plasmas *Phys. Rev. Lett.* **118** 095001
- Zhang H S, Lin Z and Holod I 2012 Nonlinear frequency oscillation of Alfvén eigenmodes in fusion plasmas *Phys. Rev. Lett.* **109** 025001
- Zhang W and Lin Z 2013 Does the orbit-averaged theory require a scale separation between periodic orbit size and perturbation correlation length? *Phys. Plasmas* **20** 102306
- Zhang W, Lin Z and Chen L 2008 Transport of energetic particles by microturbulence in magnetized plasmas *Phys. Rev. Lett.* **101** 095001
- Zhu S, Chen D, Dai Z and Wang S 2018 Numerical computation of the transport matrix in toroidal plasma with a stochastic magnetic field *Phys. Plasmas* **25** 042501
- Zonca F and Chen L 2008 Radial structures and nonlinear excitation of geodesic acoustic modes *Europhys. Lett.* **83** 35001